Lightning
Research
Group

UNIVERSITAT POLITÈCNICA DE CATALUNYA
BARCELONATECH
Escola Superior d'Enginyeries Industrial,
Aeroespacial i Audiovisual de Terrassa

Design of a field mill sensor to be used in an UAV platform for charge control research

Field Mill Sensor

Report

Degree: Aerospace Technology Engineering
Delivery date: 9-11-2020

Student: Torrent Duch, Arnau
Director: Montanyà Puig, Joan
Co-Director: Fontanes Molina, Pol

Abstract

Higher School of Industrial, Aerospace and Audiovisual Engineering of Terrassa

Design of a field mill sensor to beused in an UAV platform for charge control research

By Arnau Torrent Duch

Nowadays in aviation lightning safety efforts are focused on limiting the damage done to an aircraft when struck, and very little research on the reduction of lightning strikes has been carried out. Studies show that modifying the net electrical charge of an aircraft modifies its electrical interaction with the atmosphere and thus affecting the possibility of an aircraft triggering lightning. The ***Lightning Research Group*** at the *Universitat Politècnica de Catalunya* is currently conducting tests on an aircraft prototype with which the control of the net electrical charge in an aircraft via corona discharge is attempted. The tool to measure the amount of acquired charge is the electric field mill, and this thesis aims to design and build an electric field mill for this specific reason.

Signed declaration

I declare that,

the work in this Degree Thesis is completely my own work, no part of this Degree Thesis is taken from other people's work without giving them credit, all references have been clearly cited, I'm authorised to make use of the research group related information I'm providing in this document.

I understand that an infringement of this declaration leaves me subject to the foreseen disciplinary actions by The *Universitat Politècnica de Catalunya - BarcelonaTECH*.

Arnau Torrent Duch
Bachelor's Degree student in Aerospace Vehicles technologies

Contents

List of Tables

List of Figures

1 Introduction

1.1 Aim

The purpose of this project is to design a field mill sensor to be used in a UAV platform to investigate the control of the electric charge in an aircraft. A field mill is a sensor that measures the electric field it is exposed to, and by using multiple field mills the acquired charge of an aircraft can be measured.

1.2 Scope

The scope of the project includes:

1.2.1 Preliminary study

- Review of the Earth-Ionosphere electric system and thunderstorms.
- Review previous research on the electric charges of an aircraft, and how to control them via corona discharge.
- Review previous research on field mills used to sense the atmospheric electricity.

1.2.2 Sensor development

- Define the conceptual design: Field mill based on a modified CPU fan.
- Adapt a CPU fan into a working field mill
- 3-D print the mill's external structure

1.2.3 UAV integration

- Adaptation of the field mill to fit in the UAV.
- Add the UAV attitude information to the saved data.

1.2.4 Testing

- Conduct validation and calibration experiments at the high voltage laboratory

1.2.5 Deliverables

- Field mill built.
- Report with attachments, technical sheets, drawings and budget.

The field mill's signal conditioning electronics are **not included in the scope**.

1.3 Requirements

To complete the aforementioned scope, the following requirements must be met:

Feature	Description
1	The field mill must have **a better resolution than approximately 1 kV/m**
2	The sensor must **not make the UAV exceed its MTOW**
3	The recorded data must **include attitude information**.
4	The data measuring system must **be integrated to the existing telemetry**
5	The data measuring system must **Multiple field mills can integrated and synchronized**

Table 1.3.1: Project Requirements

1.4 Background

The Earth's atmosphere maintains an electrical potential distribution due to the electrical activity of storms across the globe, in the *global electric circuit* that's created between the Earth and the ionosphere. This means that an Earth-Ionosphere difference of potential exists. This difference of potential creates an electric field throughout the atmosphere, which varies depending on the weather conditions, and when the electric field grows to extreme levels, for example during thunderstorms, the danger of lightning strikes is no longer negligible. [17]

Modern aircraft are equipped with a wide variety of safety measures to insure that no permanent or fatal damage is inflicted upon it when struck by lightning, but they must then be grounded for a long period of time to undergo maintenance to insure the safety of the aircraft after it's been hit. Currently, among these safety measures there's little to no measures applied to *preventing* said lightning strikes. [11]

For this reason, the Lightning Research Group at the UPC and the Department of AeroAstro at MIT are currently working in several projects related to the reduction the risk of lightning inception by controlling the induced electric charge of an aircraft. Both groups are working in UAV platforms to test the control of charge by means of the production of electric coronas. To infer the amount of charge or potential acquired by the aircraft, a field mill sensor is used, but no commercial field mills are suitable for aircraft measurements.

2 State of the art

In this chapter, a brief study of multiple concepts will be done. First, the global electric circuit will be reviewed. After learning about the electric fields in the atmosphere and the factors that influence it, a review of their interaction with the electrical charge of an aircraft, and the ways to influence this interaction will be reviewed. Finally, the subject of this thesis will be reviewed: the field mill, a sensor to infer the amount of charge an aircraft acquires.

2.1 The global electric circuit

The Earth's upper atmosphere, starting at a height of 50 km and all the way up to 1000 km, solar radiation and cosmic rays ionize air particles. These ionized air particles form the *ionosphere*, which is crucial for both radio communications and atmospheric electricity, as it can be considered a conductive layer. Earth's surface, in comparison with air, can also be considered an electrically conductive layer, so in conjunction with the ionosphere, the atmosphere electrically behaves like a charged spherical capacitor.

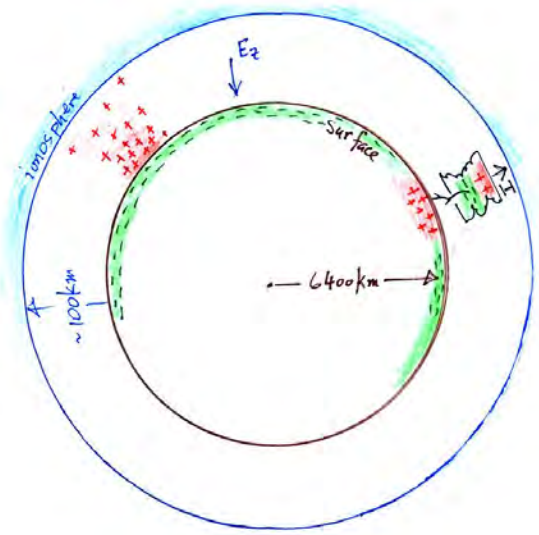

Figure 2.1.1: Earth as a spherical capacitor [17]

This behaviour causes an electric field to form in the atmosphere between the ground and the ionosphere. This electric field varies according to a wide number of factors, but the main relevant factors studied in this chapter are the weather conditions. [17]

2.1.1 Fair weather conditions

In fair weather, the ground acts as the negatively charged electrode in the capacitor, but in contrast with conventional capacitors, the positive charge is located between the ground and the ionosphere, in the air, in charged particles. In fair weather situations, most of these positive charges are found near the ground. An electric field forms between positive and negative charges, pointing towards the ground, and its value is in the order of magnitude of 100s of V/m. [16]

Air, however, is not an insulator, since charge is located in airborne mobile particles. This small but not negligible conductivity produces a weak current between ground and ionosphere, via the movement of small airborne ions.

A current flowing through a charged capacitor discharges it, but the earth-ionosphere charge difference is maintained, so there is some mechanism to transfer positive charge back to the ionosphere.

2.1.2 Thunderstorms and electrically charged clouds

The first suspects to be the way the atmosphere maintains this earth-ionosphere difference in charge were thunderstorms. Under a thunderstorm, the ground is positively charged, and the electrical field at ground level rises to the order of magnitude of 1000 V/m, and then lightning transfers negative charge to the ground. Soon, though, it was deemed to be insufficient to maintain global charge, and the consensus became that electrified clouds, thunderstorm or not, provide charging currents to the global system.

Through complex processes out of the scope of this project's investigation, thunderstorm clouds acquire different charges of different polarity inside the cloud. These differently polarized charges exist in layers within the cloud. The positive charges tend to be at the top of the cloud, while the negative charges tend towards the lower part of the cloud. [16]

2.1.2.1 Lightning

When enough charge is concentrated within the thundercloud, bidirectional channels of ionized air start to appear. These channels, called *leaders*, function as equalizers, connecting different

regions of the atmosphere. When a *leader* connects two regions of opposite charge (i.e. the opposite charge in the same cloud, or the ground), current flows from one region to the other: a lightning strike. [18]

Lightnings carry positive charge to negative regions, so when the ground is struck by lightning, the positive charge it has acquired with the fair weather current is discharged back into the atmosphere, helping maintain the global electric circuit.

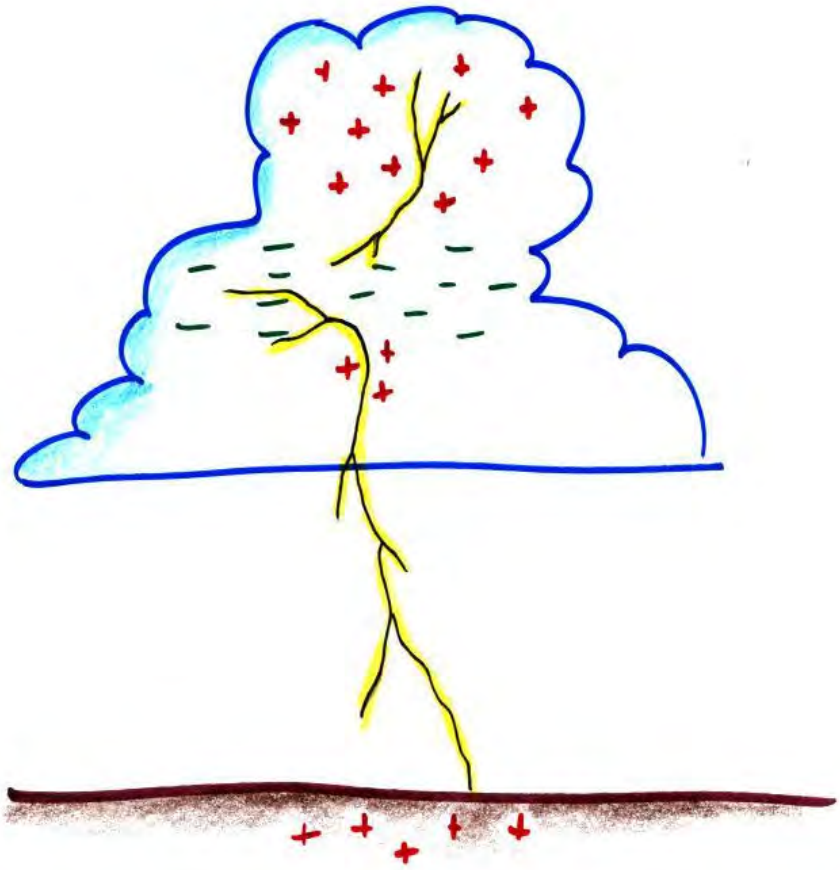

Figure 2.1.2: General structure of lightning [18]

Now that we know why, how, and the relevance of lightning strikes, let us consider its impact in current air travel.

2.2 Charges in an aircraft

Now let's consider an aircraft flying through the atmosphere. If this aircraft has non negligible electric charge, either due to natural causes, or due to artificial charge control, the electric field polarizes this charge in positive and negative ends, and magnifies the electric fields in its extremities. Since positive leaders have a lower threshold of propagation, meaning that with the same charge a positive leader is always created before a negative leader. To maintain charge neutrality in the aircraft, the negative electric field in the aircraft increases to balance out the increasing positive charge due to the leader. This, in turn, allows for the appearance of negative leaders in the negatively charged part of the aircraft. If both positive and negative leaders connect to the cloud and the ground/the cloud itself, as was seen in the previous chapter, lightning strikes. These strikes are called *aircraft-trigged lightnings*. [11]

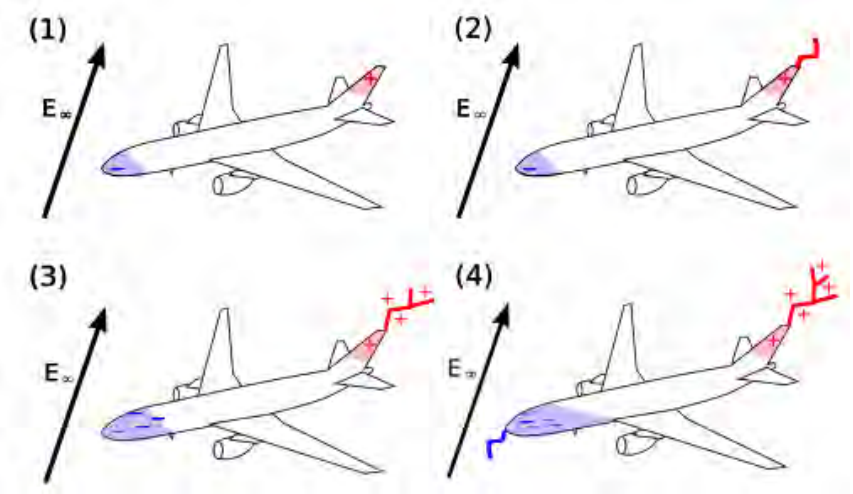

Figure 2.2.1: Process through which an aircraft triggers lightning [11]

When an aircraft is hit by lightning, the current flows through the outer metallic layer, excluding any aircraft systems, payload or passengers from its potential damage. Newer aircraft made from composite materials have metallic meshes around its outer layer, but damage can still be done in places with poor conductivity.

2.2.1 Effect of an aircraft's net charge in aircraft-triggered lightning

To better understand aircraft-triggered lightnings, a laboratory experiment was performed [11]. This experiment involved a small-scale model of an aircraft which served as the means to study the positive leader inception, the first stage of lightning.

To do so, the conductive aircraft model was placed between a high voltage electrode and a grounded electrode to generate the electric field. The high voltage plate was then put through charge curves which increased its voltage up to a maximum value in a set time. The experiment

consisted in charging the conductive aircraft model and finding the electric field value at which a positive leader forms. Each curve is slower than the last. The results of the experiment are shown in the graph below:

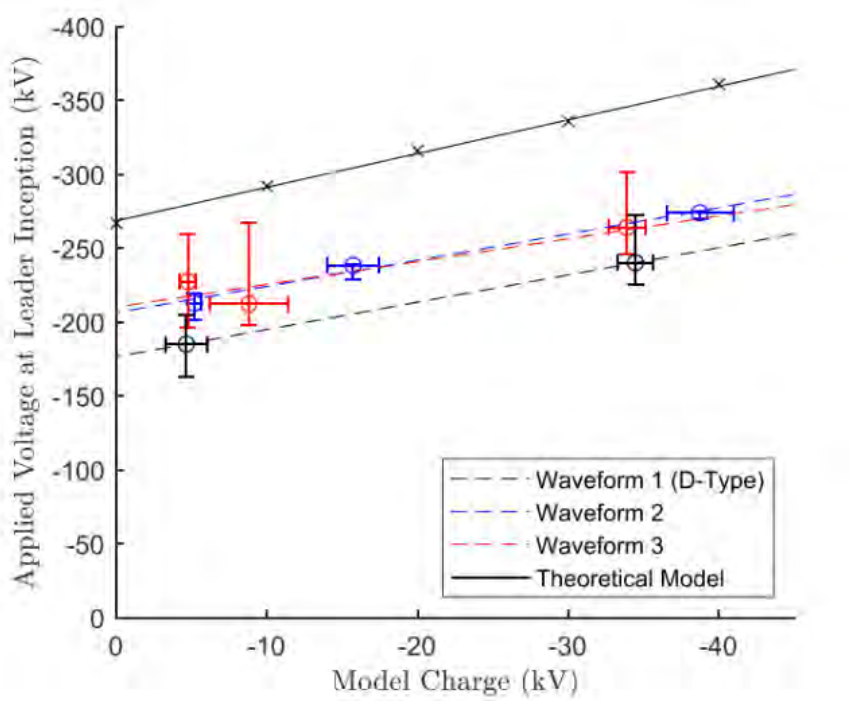

Figure 2.2.2: Positive leader inception experiment results [11]

Figure 2.2.2 shows the relation between the electric field value at which a positive leader was formed and the amount of net charge in the model aircraft. The faster the rise of the electric field, the less value of it is required to allow for positive leader inception. Further slowing down the charge rises the positive leader threshold, but slightly decreases the impact of the aircraft's net charge. The tendency is clear: negative charge increases the electric field threshold for positive leader inception, but the speed at which the electric field changes around the aircraft must also be taken into account.

2.2.2 Artificial charge control on an aircraft using corona discharge

For a conductive body floating mid-air to change its charge, positive or negative charges must be emitted from it. A study performed by **UPC's *Lightning Research Group*** in collaboration with **MIT's *AeroAstro*** had as an objective to study the possibility of an aircraft's charge control system by emitting electric coronas from a live wire.

When a conductor is charged positively with high voltage, a glowing layer will appear near it. This glowing layer is called the *corona discharge*. As voltage rises, this corona discharge appears as a repetitive burst. If the conductor is negatively charged, this burst has a consistent

period, and if it's positively charged, the burst is more unpredictable and erratic, and when the voltage increases further, the burst becomes a permanent glow. [13]

In the permanent glow corona discharge regime, positive ions form near the conductive wire. These ions are then convected away from the body by the wind, charging the aircraft negatively. In turn, the acquired negative charge in the body of the aircraft attracts the positive ions in the air, so as the negative charge increases, the number of positive ions escaping the aircraft's influence decreases until an equilibrium point is reached.

Further experiments in the wind tunnel proved this method to work, and proves that the faster the aircraft flies, less current is needed to decrease its charge and the more negative the aircraft charges. [6]

2.3 The field mill

A field mill is a rotating vane-style instrument designed to measure static electric fields. The field mill uses electrodes which, when exposed to a static electric field, acquire electric charge. This sensing electrode is then periodically covered and uncovered by a shielding electrode connected to ground. This periodical change in induced charge at the sensing electrodes generates a current, which when passed through an impedance can be transformed into a difference in potential, which can be measured.

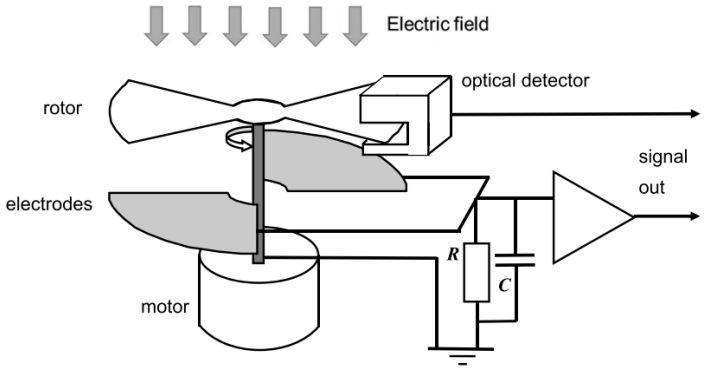

Figure 2.3.1: General structure of a field mill [8]

Figure 2.3.1 shows the typical structure of a field mill. The rotor is the shielding electrode which is connected to ground, the sensing electrodes are fixed, and the signal from the sensing electrodes is then processed. The induced current on the sensing electrodes is extremely faint and noisy, so to properly collect relevant data from a field mill significant filtering and amplifying is necessary for the post-process of the gathered data.

The aforementioned general structure includes an optical detector which serves as a phase lock, which means the data is sampled at each point in the rotation every time. This way instead of dealing with a repeating pattern the post-processor only has to compare the fixed value at each rotation.

For the field mill designed in this thesis, no phase lock will be implemented, and instead the signal processing electronics returns the RMS value of the output signal's pattern.

A field mill is usually used to measure the atmospheric electric field from the ground. This information is then used as a thunderstorm warning system, and as a safety indicator for sensitive events. The best example of an atmospheric electricity-sensitive event is a rocket launch. SpaceX's Falcon 9 rocket launch weather criteria includes a maximum field mill reading for a safe launch. [12]

The application of the field mill this thesis is interested in, however, is the option of measuring the acquired charge of an aircraft.

2.3.1 Measuring the acquired charge of an aircraft

Let's consider an aircraft flying through the atmosphere. If this aircraft was to have two field mills, one pointing skyward and one pointing to the ground, the two values of the electric field measured by each mill could be compared.

When the aircraft is in the ground, before takeoff, it is safe to assume that its charge is zero, given the contact it has with the ground. The lower field mill then measures an electric field of 0, since the aircraft and the ground have the same charge. At the same time, the upper field mill measures the electric field of the atmosphere.

After takeoff, and after the aircraft acquires charge either by natural or artificial means, the upper field mill's reading is lower, because the "ground" voltage in the field mill is shared with the grounding of the aircraft, so the ground reference now has higher voltage. The lower field mill also has a different reading than on the ground. The lower field mill measures a higher field value than on the ground, for the same reason as the upper field mill.

By comparing the two readings it is now possible to calculate the acquired charge of the aircraft, as well as the atmosphere's electric field. The lower field mill reading corresponds to the electric field caused by the acquired charge in the aircraft, and the difference between the upper field mill reading and the lower field mill reading is the atmosphere's electric field.

3 | Field mill initial parameters

The objective of this project is to build a working light-weight field mill from a CPU fan. Before starting the design of the structure or the internal software, certain general design decisions must be made. These include: the sensitivity, the size limitations, the materials used as electrodes, and the fan model to use. In this chapter, these initial parameters will be computed.

3.1 Size

The field mill is to be used in the study of artificial charge control in an aircraft. To be more precise, the device is to be mounted on an experimental UAV conditioned to allow for charge control. The model of the used UAV is the *MAJA XL*, with a wingspan of 2,2m and a total length of 1,2m. A study of which location is best for the field mill to be integrated in the aircraft is outside the scope of this project, but the external structure should still fit in the main fuselage. Henceforth, taking into account the total fuselage width which is 10 cm, the smallest dimension of the field mill should be no larger than approximately 6 cm to allow for proper integration.

Figure 3.1.1: Picture of the UAV [2]

The field mill is installed in the distinctively smoother surface at the top and bottom of the aircraft.

3.2 Sensitivity

This section pretends to be the basic preliminary calculation to narrow down the possible design parameters that fulfill the sensitivity requirements.

When a field mill is exposed to the atmosphere, which behaves as a capacitor, the static sensor electrodes see a change in the exposed area to the atmosphere. This time-varying capacitance induces current through the sensor electrodes, which in turn becomes a difference of potential when the current passes through an impedance. This difference in potential is the measured magnitude which is indicative of the electric field in the atmosphere. [14]

The charge in the sensing electrodes is proportional to the exposed area:

$$q(t) = \varepsilon_0 E a(t) \tag{3.2.1}$$

Where a(t) is the exposed area, ε_0 is the permittivity, and E is the electric field, supposed constant due to the rate at which the aircraft moves between different intensities of electric field in the atmosphere. The current in the sensing electrode can then be derived from the induced charge:

$$i(t) = \frac{dq(t)}{dt} \tag{3.2.2}$$

The area variation in steady state and constant rotation of the shielding electrodes changes linearly, so its derivative is reduced to the variation of charge (area) during the rotation period. Henceforth, the maximum induced intensity at the sensing electrodes is the total increase of area in half a period, which is the time it takes for the blocked electrode to be completely unblocked:

$$I_{max} = \frac{\varepsilon_0 E A_{max}}{T/2} \tag{3.2.3}$$

Passing this current through an impedance allows for the measuring of the difference in potential. In this project, the impedance consists of a certain resistance R, but the sensing electrode with the grounding electrode forms a capacitor with the air as the dielectric. This capacitor can be assumed to have very high capacitance since it boasts high surface area, high

permittivity and low distance between the two conductive plates. When the induced current is positive, this capacitor charges over time, and when the intensity then flips to negative, the capacitor discharges, so the expected output of the field mill is a triangular wave.

. A summary of the time-varying magnitudes is shown in figure 3.2.1

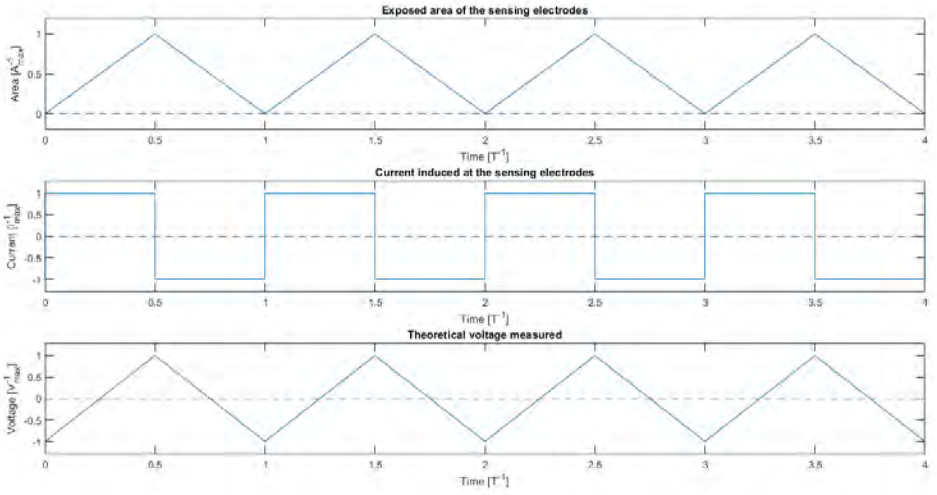

Figure 3.2.1: Exposed area, induced current, and expected measured voltage of the field mill

In figure 3.2.1 the maximum value of voltage differential, V_{max}, has to be the same as the voltage differential in the resistor with which the output is measured. To calculate said voltage, it is possible to calculate it using *Ohm's law*, which states that $V = IR$:

$$V_{max} = 2f\varepsilon_0 E A_{max} R \tag{3.2.4}$$

As equation 3.2.4 shows, the sensitivity of the field mill increases with its area, its rotation frequency, and the resistance used to measure the current. The total area of the field mill is limited by the size, the frequency is limited by the CPU fan used, and the maximum voltage is limited by the electronics, since too high voltage after filtering and amplifying the signal could damage some electronic components in the circuitry.

3.3 CPU Fan

In this project the fan was provided by **UPC's *Lightning Research Group***, but its properties will be discussed.

The CPU fan model used in this project is the **Noctua NF-P14s**. At the core of this fan is an electric motor which, after dismantling the fan, will be used. Nevertheless, the basic properties

of the fan can be extrapolated and approximated as the field mill's properties.

The fan has a PWM controlled brushless DC motor with a maximum rotation speed of 1200 RPM. Its nominal input voltage input is 12V, with a power input of 0.96W. The motor also already includes its microcontroller, meaning that it only has 4 pins: Input V_{in}, GND, RPM sensor, and PWM input.

According to *Noctua*'s PWM modulation datasheet, the fan's RPM sensor generates two pulses per each rotation. [10]

Pictured below is the disassembled fan:

Figure 3.3.1: Disassembled fan: on the left, the rotating elements. On the right, the static elements

Figure 3.3.1 clearly shows the electric motor is an outrunner, meaning that the stator is inside the rotor. The four radially assembled coils interact with the single magnetic ring in the fan, making it spin.

With all the initial conditions exposed, the design process starts. It will be separated in two main parts: The software development, and the design of the outer structure.

4 | Software development

In this chapter, the process of designing a control system for the extracted DC motor, as well as the attitude information gathering. To control the DC motor and gather the attitude information, an Arduino board is chosen as the electronics platform. The Arduino codes developed in this thesis can be found in the report attachments.

Arduino is a corporation that commercializes open-source prototyping electronic boards based on easy-to-use hardware and software. It also uses its own IDE and programming language, which is intuitive and relatively simple [1]. In this thesis only the key aspects of Arduino that allow for integrating a control system will be explained. These key aspects are:

- PWM modulation in certain pins
- Built in interruptions

The first aspect is really intuitive. Arduino has a function within its own language which sends out a PWM signal from one of its pins. This signal is modulated with a duty cycle ranging from a flat LOW output to a flat HIGH output. LOW and HIGH outputs in an Arduino board mean a 0V output for LOW, and a 5V output for HIGH. To send out a PWM signal the function *analogWrite(P,D)* is used. In this function, P is the output pin which sends the signal, and D is the duty cycle of said signal. This duty cycle influences the ratio of time at which the output signal is HIGH versus LOW. To set the speed input of the motor, the PWM pin is connected directly to Arduino, and then an output signal is sent.

The next aspect is the interruptions. To be able to have interruptions in an Arduino program, the interrupt must first be attached to a pin and given a condition. Once the interruption is set up, when the condition is met in the pin, an interrupt happens. During this interrupt, any process being performed by the Arduino board is paused and the lines of code in the interruptions are performed. To read the signal from the RMP output sensor, this interruption utility is used.

To set up the interruption, the Arduino function *attachInterrupt(P,Function,Condition*. "P"

is the pin which receives the interruption signal, This pin is usually accompanied by the *"digitalPinToInterrupt(P)"*, which translates from the digital pin to the appropriate interruption label within the board. Interruptions, which range from data transmissions from a computer, to the pressing of the reset button in the board, have a distinctive label in the board micro-controller which identifies each situation and gives every interruption the appropriate priority. "Function" is the name of the function which will be run during the interruption, and "Condition" is the behaviour of the entering signal which will trigger an interruption. These conditions are:

- **LOW**: The interruption is triggered when the pin is LOW
- **CHANGE**: The interrupt is triggered when the pin changes value
- **RISING**: The interruption is triggered when the pin goes from LOW to HIGH
- **FALLING**: The interrupt is triggered when the pin goes from HIGH to LOW

As mentioned in section 3.3, the DC motor's RPM sensor sends two pulses per rotation [10]. The output signal waveform is shown below:

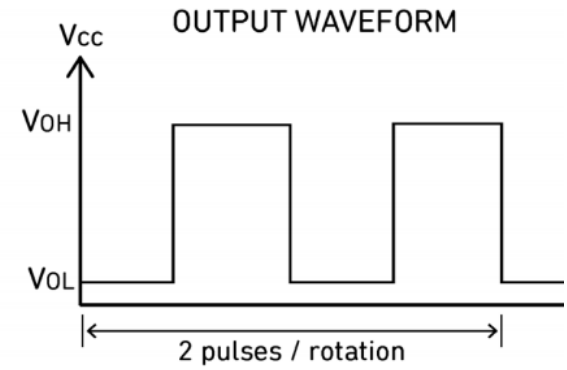

Figure 4.0.1: RPM sensor output waveform

Based on the waveform in figure 4.0.1, it is clear that the actual value of the RPM reading is not sent out and instead it has to be computed from the frequency of the pulses. With the use of interrupts, this frequency calculation is simply a time difference between interrupts.

The waveform changes value four times throughout a rotation. It rises twice, and it falls twice. If the interruption is attached to the "CHANGE" condition, an interruption is triggered twice as often as if it was attached to a "RISE" or "FALL" condition. In the code to be run during the interruption, it is beneficial to reduce the computation load as much as possible. So, the function inside the interruptions to calculate the frequency of the electric motor only has as an objective to save the time difference between interruption triggers.

To calculate the time difference, first it is necessary to ensure that the time difference will be calculated every two interruptions. A logic variable is used to ensure that every first interruption will save a time and the second will compute the difference. To save and subtract time, the function "*millis*" proves useful, since it returns the amount of milliseconds that have passed since the board turned on. Then, outside of the interruption, the motor's RPM regime is calculated as follows:

$$w_{motor} = \frac{60}{2(t_{PulseFinish} - t_{PulseStart})} \quad [min^{-1}] \tag{4.0.1}$$

4.1 Control of a DC motor

A DC motor can be considered a first order system, which can be modeled using a first order differential equation. When this system is excited with a certain input, it has a characteristic response, as shown below. The following figure was plotted by connecting the V_{in}, GND and RPM sensor pins, but leaving the PWM control disconnected. The RPM signal sensor was read using an Arduino Mega 2560.

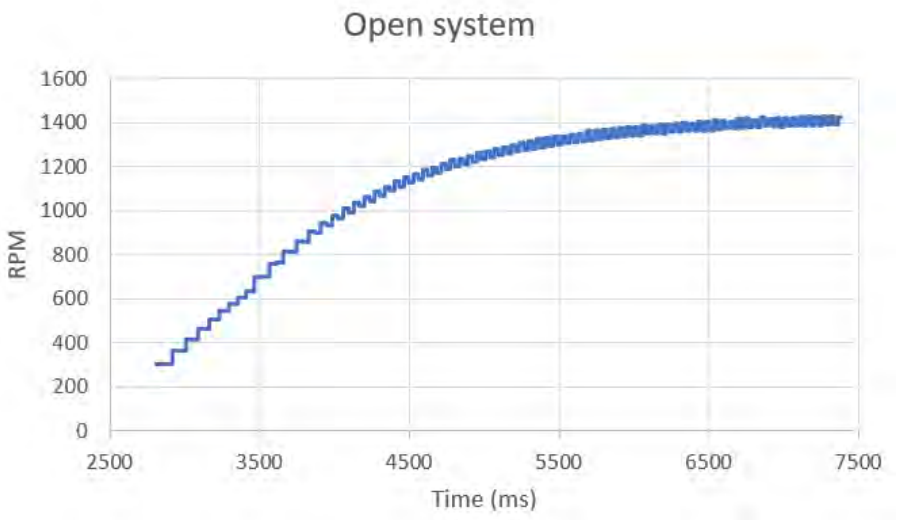

Figure 4.1.1: Response of the system when no control input is sent.

This response is called the first order open-loop response. The system simply reaches its maximum RPM in approximately 5 seconds. This behaviour is not interesting for this project, so there's a need for a control system.

The first part of controlling the open-loop system is to close the loop. Using the RPM sensor, it is possible to feed the information back into the program. By comparing the desired output and the actual output, an error is calculated. Here, the variety of controller options opens up.

If the input signal is changed proportionally to the error, a *Proportional "P" controller* is in effect. The *P controller* is the most basic of control systems, but it has shortcomings. Mainly, because it is unable to correct non-linearity in the system. Also, when introduced into a noisy system the rapidly changing error can prevent the desired output from reaching stability.

In addition to proportional control, it is possible to change the input signal by also taking into account the variation of the error over time along with the proportional influence. The *proportional-derivative "PD" controller* solves the non-linearity error, since it counteracts the tendency of the error. The main downside to using *PD controllers* is the noise in the system. As definition, noise consists of rapid variations at much higher frequencies than the measured magnitude. As such, its derivative quickly grows out of control, since instantaneous error has very high derivative value but very little duration and relevance in the system.

A solution to the *PD controller*'s issues is to instead of using the error's derivative, to use its accumulation. By integrating the value of the error in a *proportional-integrative "PI" controller*, the non-linearities of the system can still be counteracted, and the influence of rapidly-changing instantaneous error becomes negligible.

It is also possible to combine the three previous control schemes into a *"PID" controller*. However, given the influence of the aforementioned derivative part of the controller, the final control method is the ***PI controller***.

4.1.1 PI Controller

When the loop is closed, the block diagram of the system is as follows:

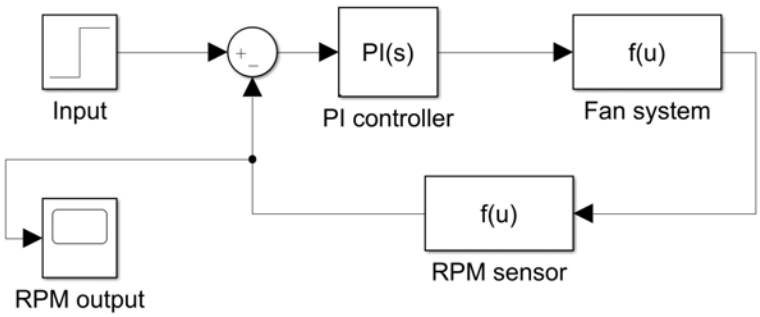

Figure 4.1.2: Block diagram of the closed-loop system

To implement such a control structure, and since the fan's control is via PWM-Pulse Width Modulation, Arduino was chosen as the electronic platform.

4.1.1.1 PI Control via Arduino

To implement a controller, the duty cycle sent to the motor is modified based on the error. This error is calculated by subtracting the target RPM value to the current RPM value received from the sensor. The duty cycle is modified as follows:

$$D = D + K_P\varepsilon + K_I \int \varepsilon \tag{4.1.1}$$

In this equation, D is the duty cycle, ε is the error, and K_P and K_I are the PI controller's proportional and integrative coefficients. These coefficients dictate the system's behaviour.

Since the error doesn't have a set function and changes each pulse of the DC motor, it cannot be analytically calculated. The integral must be discretized every two pulses. As the integral is the value of the area under a curve, the trapezoid method is used to approximate the curve of the error. Once reduced to trapezoids, the area under the curve can be easily calculated. An example of the trapezoid approximation method is shown below:

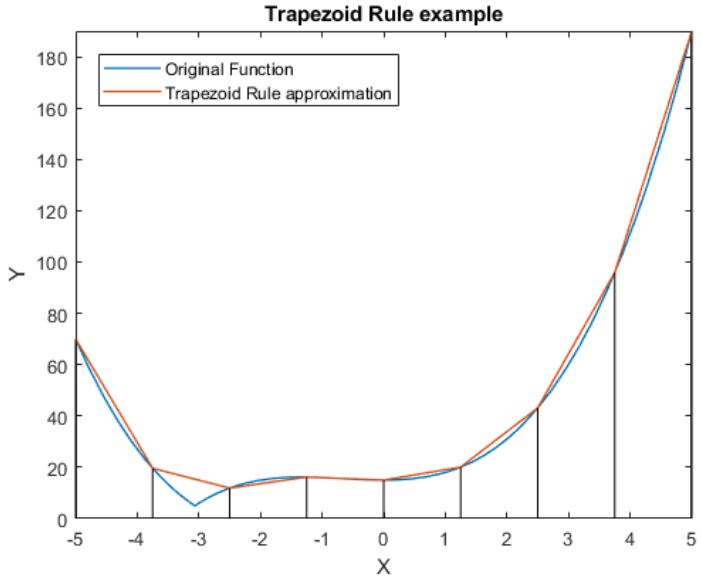

Figure 4.1.3: Trapezoid approximation method

To calculate the area of a trapezoid the average side length is used, henceforth it is imperative to know both the current error and the previous instance of error. Naming the error as ε, the discretized integral can be calculated:

$$\int \varepsilon = \frac{\varepsilon_{Current} + \varepsilon_{Previous}}{2}\Delta t \tag{4.1.2}$$

Where Δt is the discretization time. This time differential is the elapsed time between instances of error, so it is already known: it is the time between interruptions calculated in a previous

section. Substituting the integral at the duty cycle calculation:

$$D = D + K_P \varepsilon_{Current} + K_I \frac{\varepsilon_{Current} + \varepsilon_{Previous}}{2} (t_{PulseFinish} - t_{PulseStart}) \tag{4.1.3}$$

The next step is to determine the K_P and K_I coefficients. The process with which the coefficients are found is called ***PI tuning***

4.1.1.2 PI tuning

To tune a *PI controller* multiple options arise. If the system has a known behaviour and has been properly mathematically modeled, which means that it can be simulated, there are known formulae to find the appropriate coefficients to achieve any behavioural goal. If the system cannot be properly modeled, empirical methods can be used to find the coefficients that allow for stability and precision. The method used in the tuning of the PI for the DC motor system is an empirical one, since for our purposes (control and stability) is enough, and it is much simpler. The method used is the ***Ziegler-Nichols*** method.

Ziegler-Nichols method [15]

This tuning method is based on finding a K_P that meets a certain condition while K_d and K_I are 0. The "*ultimate* K_P", as it's called, is the lowest value of K_P at which the system is not stable. To find it, a low value of K_P is initially set. Then, after checking the behaviour of the system, the K_P is slowly increased, until the *ultimate* K_P is found. At this K_P the system oscillates with constant amplitude and constant period.

Once the *ultimate* K_P and its oscillation period are found, the *Ziegler-Nichols* method has relations between the K_{Pu}, the K_P, the K_I and the period T_u.

Control type	Kp	Ki	Kd
P	0,5 K_{Pu}	0	0
PI	0,45 K_{Pu}	0,54 K_{Pu}/T_u	0
PD	0,8 K_{Pu}	0	$K_{Pu}T_u/10$
PID	0,6 K_{Pu}	1,2 K_{Pu}/T_u	3 $K_{Pu}T_u$ / 40

Table 4.1.1: Ziegler-Nichols relations table

By using this method, the only requirement for tuning the PI controller is to find the K_P at which the system oscillates. The behaviour of the oscillating system is found by trial and error.

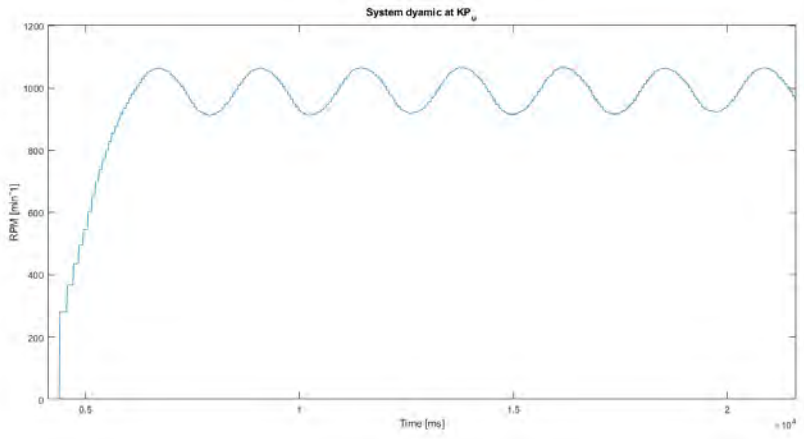

Figure 4.1.4: The system oscillating at the K_{Pu}

Figure 4.1.4 plots the response over time of the motor when oscillating under K_{Pu} conditions. The system has a transient state when started, lasting approximately 6 seconds. Then the system enters a periodic oscillation state with a period of 2,38 seconds. The K_P that produces this oscillation is 0.04. According to the *Ziegler-Nichols* method, the K_P and K_I coefficients for this system are:

$$K_P = 0.45K_{Pu} = 0.018 \tag{4.1.4}$$

$$K_I = 0.54\frac{K_{Pu}}{T_u} = 0.0091 \tag{4.1.5}$$

Implementing these coefficients in the Arduino controller changes the system's behaviour:

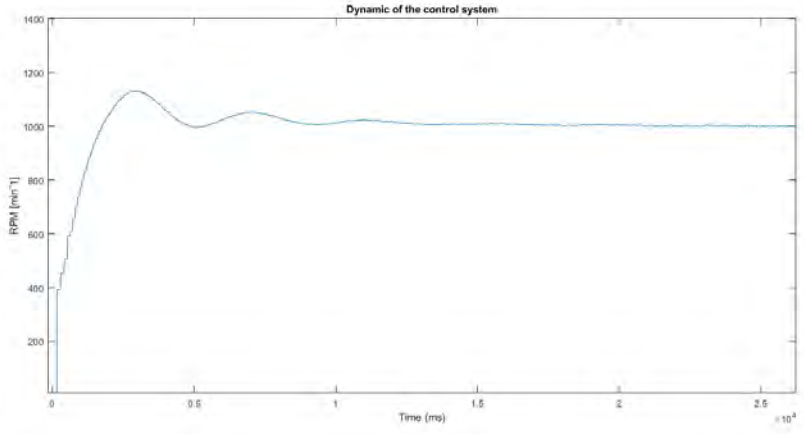

Figure 4.1.5: Response of the controlled system

In the previous figure 4.1.5, like in the situation with the K_{Pu}, the system shows a transient state at start, with certain overshoot, but after 12-13 seconds the system achieves stability in a permanent state at the target RPMs. Even in the event of a perturbation in the system, the controller makes the appropriate corrections.

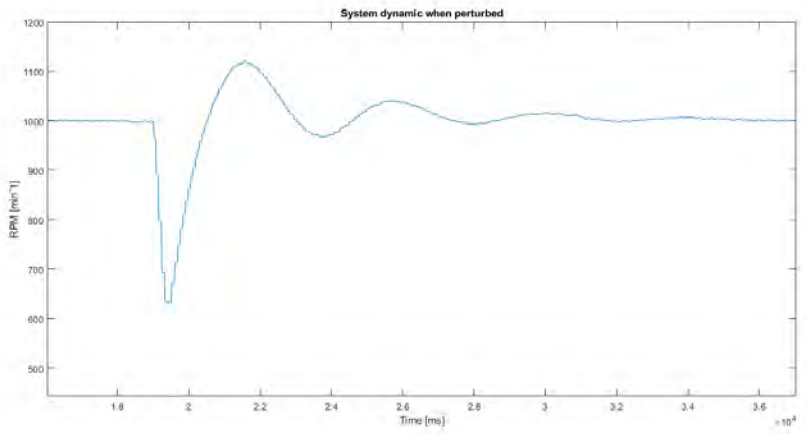

Figure 4.1.6: Response of the controlled system when perturbed

This figure shows the response of the system when artificially perturbed. In this case, the perturbation was done by touching the fan and slowing it down. After the perturbance the motor accelerates to return to the target rpm regime. When it reaches it, it has some overshoot, and after approximately 10 seconds the system is back to its stable steady state.

As per the requirements of this thesis, the speed synchronization of two field mills is necessary.

4.1.2 Synchronization of multiple motors

To synchronize multiple motors, the same method of control is employed to control each motor. The difference is that the target RPM value of the motors has inter-dependancy now. To synchronize two motors, one of the motors is the ***Master*** and dictates the RPM of the system (and has as a target the required RPM regime for the field mill), and the other is the ***Slave*** motor, which has as target RPM the current RPM value of the *Master* motor.

In Arduino, another interruption must be set up, and the same process as with the first motor is followed. A flag variable is introduced, and every interruption this flag variable is switched to allow for the recording of the initial pulse time and the final pulse time. A new possibility arises: two interruptions triggering at the same time. When that happens, the second interruption is buffered, so when the code inside the first interruption ends, the main Arduino program is not unpaused and continued, but instead the code inside the second interruption runs. The Arduino function used to compute the time is not incremented inside interruptions, so a certain imprecision can appear when multiple interruption systems are in play.

The diagram of the dual motor system is as follows:

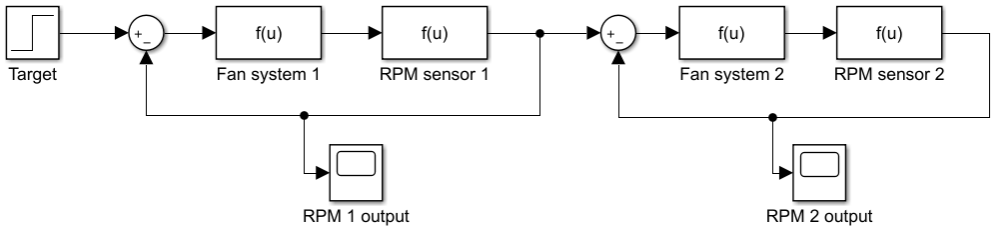

Figure 4.1.7: Block diagram of the dual motor system.

The figure is essentially the same structure as figure 4.1.2, but in the second instance of the closed-loop structure its input is the output of the single closed-loop structure.

The *PI controller* of the second motor must still be tuned in the same way as the first motor. For this motor, the values are summarized below:

- K_{Pu}: 0.16
- T_u: 2.036 s
- K_P: 0.072
- K_I: 0.0424

When both fans are active and controlled, their combined dynamic is as follows:

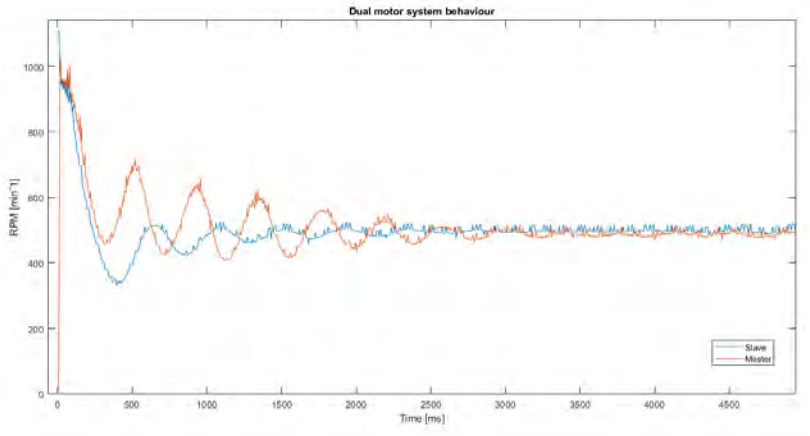

Figure 4.1.8: Behaviour of the synchronized motors

In the figure 4.1.8, the initial spike and overshoot of the system is due to the way Arduino receives data upon being turned on, because while receiving the PC's transmission with the program the duty cycle of the fans is undetermined, so the fans spin at max speed. After the program has been properly received and started, the system then goes through a transient state of about 3 to 3,5 seconds before reaching steady state stability. It is also clear to

see that there is some undulation in the steady state signal of the master motor. This undulation meets *Ziegler-Nichols*'s criteria of stability. The slave motor, however, is much more stable. The presence of noise is also evident in the system. This noise is probably due to interactions between the interruptions, and due to the way the time in "*millis()*" is saved. When a portion of a millisecond has past, *millis()* rounds the value up or down, henceforth generating discontinuities in the calculated RPM value.

4.2 Aircraft attitude information gathering

To obtain the attitude information of the aircraft a special sensor is used. This sensor, an ***Intertial Measurement Unit*** or IMU for short, measures the orientation in each axis of a body using accelerometers, gyroscopes, or magnetometers. For this project the IMU **Adafruit BNO055** is used.

4.2.1 Adafruit BNO055

The Adafruit BNO055 is a small light 9-DOF sensor. The particularity of this sensor is that in its printed circtit board PCB it includes the algorithm to merge all the information of its sensors into simple outputs. For example, if asked for the XY orientation, instead of the reading of each sensor the BNO055 outputs a single number ranging from 0 to 360º, so the information is available without any additional calculations. The available data from the sensor is: the **Absolute Orientation**, the **angular velocity vector**, the **Acceleration Vector**, the **magnetic field strength vector**, the **linear acceleration vector**, the **gravity vector**, and the **temperature**. [5]

As shown in figure 4.2.1, the sensor has a wide variety of possible outputs, but there's not enough pins in the PCB for such an amount. The reason behind the small number of output pins is the use of the ***I2C protocol***.

4.2.2 I2C protocol

The I2C protocol is a serial communication bus which connects a *master* device with multiple *slave* devices. It only requires two wires, one for the clock signal "**SCL**" and one for the transmission of data "**SDA**". When multiple devices are connected via I2C, each device is given a unique address which can be modified by the *master* device. A single device, for example the *BNO055* IMU, can have multiple addresses within it. Each address points to different available sensor data the sensor can provide, as mentioned in section 4.2.1

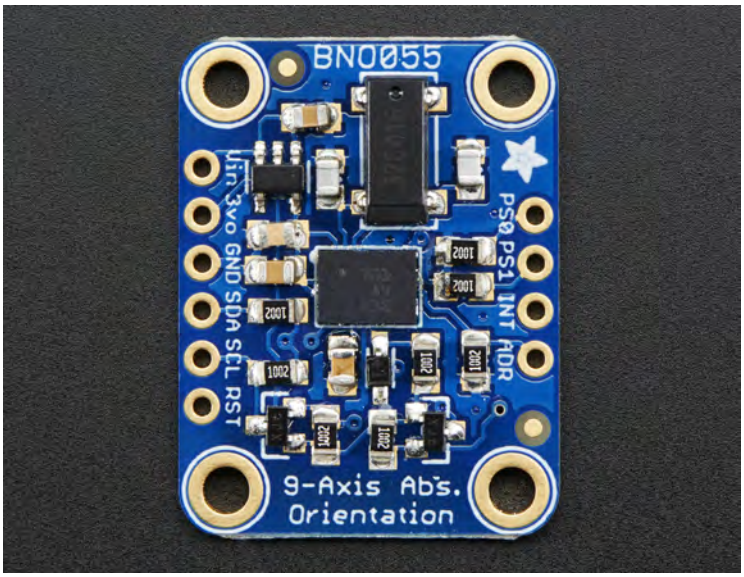

Figure 4.2.1: Adafruit BNO055 IMU

The clock signal is sent by the *master* device and it synchronizes all other devices connected via I2C. Then, the *master* device sends a signal through the SDA pin. This sent signal is a compilation of bits: the address of the *slave* device with which to communicate, followed up by a bit with the communication intention (to read or to write), a validation bit, and then the data. This data sent by the *master* is usually the *slave*'s available data which to read or write [4]. An example of a I2C transmission can be found below:

Bit	**0**	**1**	**2**	**3**	**4**	**5**	**6**	**7**	**8**				**0**	**1**	**2**	**3**	**4**	**5**	**6**	**7**	**N**
Value	0	1	1	0	0	1	0	0	1				0	1	1	1	0	0	1	0	0
	Address							**R/W**	**ACK**				**Data (7 bits)**							**NACK**	**STP**

Table 4.2.1: Example of a I2C transmission

In table 4.2.1 the 7th bit in the address transmission is the Read/Write determination, which dictates what's done with the accessed data, and the 8th bit or "Acknowledge" bit serves as validation that there are no errors in the communication. When the *slave* sends its response, the last bit before the end of the transmission must be the opposite of the "Acknowledge bit" to validate proper communication.

Using this technology, the transmission of the data of the ***BNO055*** IMU is simplified to an existing communication protocol which has libraries in Arduino that allow for intuitive communication. Furthermore, the sensor's manufacturer, ***Adafruit***, has a library of its own to further simplify the reading of the measurements of the sensor.

5 | Hardware development

In this chapter the connections in the Arduino board, the process through which the external structure for the field mill is designed and the final design will be discussed.

5.1 Arduino board circuits

Two Arduino circuits have been built in order to carry out the programs described in the previous chapter. These circuits were built on protoboards, which are not permanent and allow for modification once built. To properly integrate the arduino circuits they should be soldered onto a proper board. The circuits built are:

- DC motor control and synchronization
- Attitude sensor reading

5.1.1 DC motor control and synchronization

The motor control and synchronization program has two inputs and two outputs.

- **Inputs**: The RPM sensors of both motors.
- **Outputs**: The PWM signal.

The output signal from the RPM sensor in the motor is fairly weak and the Arduino board's digital logic pin doesn't recognize the sensor's signal and doesn't trigger interruptions. To solve this issue, a **pull-up resistor** is used to increase the signal's intensity to the point that Arduino recognizes it. [10]

A **pull-up resistor** is used when part of the signal of the logic state isn't clearly defined. For example, in the case of the DC motor, the sensor's pulse goes from ground to a certain voltage

level. The ground state is clearly a logic LOW state, but when the sensor is supposed to be HIGH, the value isn't certain. In this case, the HIGH signal is floating somewhere between what Arduino recognizes as LOW and HIGH, causing irregularities in the signal preventing its proper processing. In case of the Arduino, the pull-up resistor is connected between the board's 5V power supply and the sensor. When the incoming signal is connected to ground and therefor a LOW, the input pin is shortcut to ground too, recognising the signal as LOW. When the incoming signal is a certain voltage, the input pin detects the 5V power supply through the pull-up resistor, so it recognises this signal as a HIGH logical value.

The value of the resistor can be found by trial and error. In the case of this circuit, the resistor value chosen was 10 kΩ.

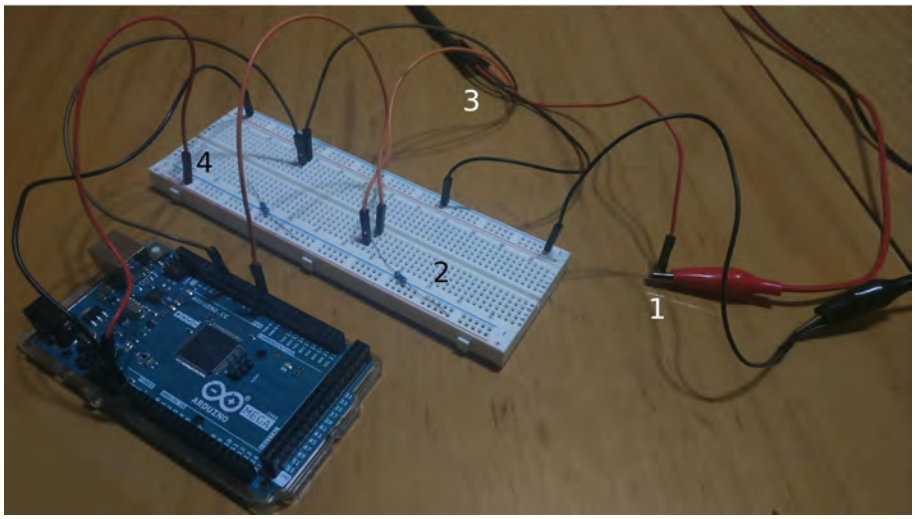

Figure 5.1.1: Built motor control circuit

In the figure 5.1.1 the circuit to achieve control in one DC motor is shown. In the figure, several parts of the circuit are enumerated:

1. Red and black cables coming from the red/black pincers are the 12V power supply, which power the motor
2. The pull-up resistor which connects the Arduino's 5V power supply with the PRM sensor signal (orange wires).
3. The motor's 4-pin connector. Power supply (Black wire for GND, red wire for 12V), RPM sensor (orange wire) and PWM input (brown wire).
4. Arduino's 5V power supply (red wire).

It is important to note that the protoboard connects the two outer rows in each side horizontally, and the rest of the columns vertically. In this protoboard there are two pull-up resistors because

it was used to synchronize the two motors. The second motor is not included for clarity reasons, because it's the same circuit.

5.1.2 BNO055 sensor reading

Because of the I2C communication protocol explained in section 4.2.2, the communication between the sensor and the Arduino is reduced to a total of four cables:

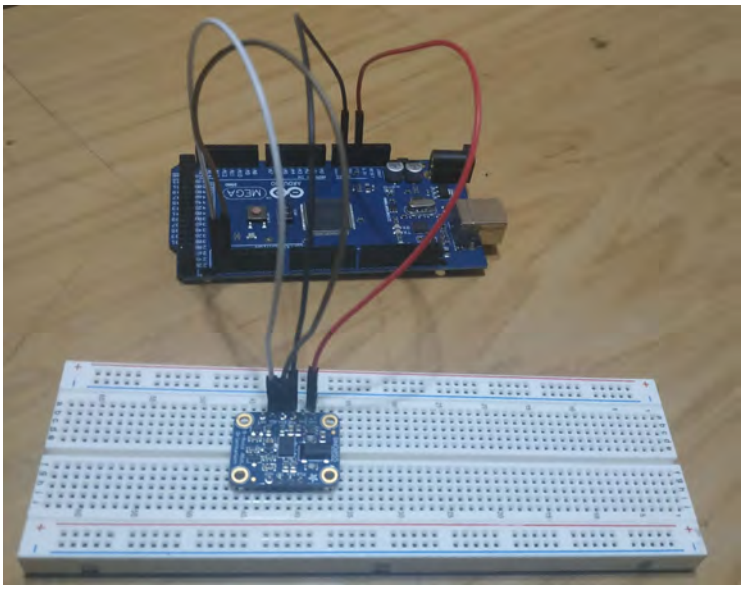

Figure 5.1.2: Connection between the BNO055 sensor and the Arduino board

Figure 5.1.2 shows this simple connection. The only necessary wires are:

- **Power supply**: Red/black wires
- **I2C SCL**: White wire
- **I2C SDA**: Brown wire

The two circuits can be implemented at once, along with the two different programs, but for clarity they have been separated.

5.2 Structure design for the field mill

The structure of the field mill has three main purposes:

1. House the DC motor
2. House the sensing and blocking electrodes
3. Allow for integration in the aircraft

The first step is to know the measurements for the dismantled DC motor to be able to design a new casing for it.

5.2.1 Brushless DC motor casing

The dismantled motor consists of two main parts: a rotor and a stator. The rotor consists of a metallic ring surrounding a permanent magnet, which is rubber-like. The stator has four coils arranged radially, but with permanent magnets at the end. The spinning part of the fan has the axis embedded in its center, and the bearing goes through the center of the stator.

A general diagram of the size of both parts is shown below:

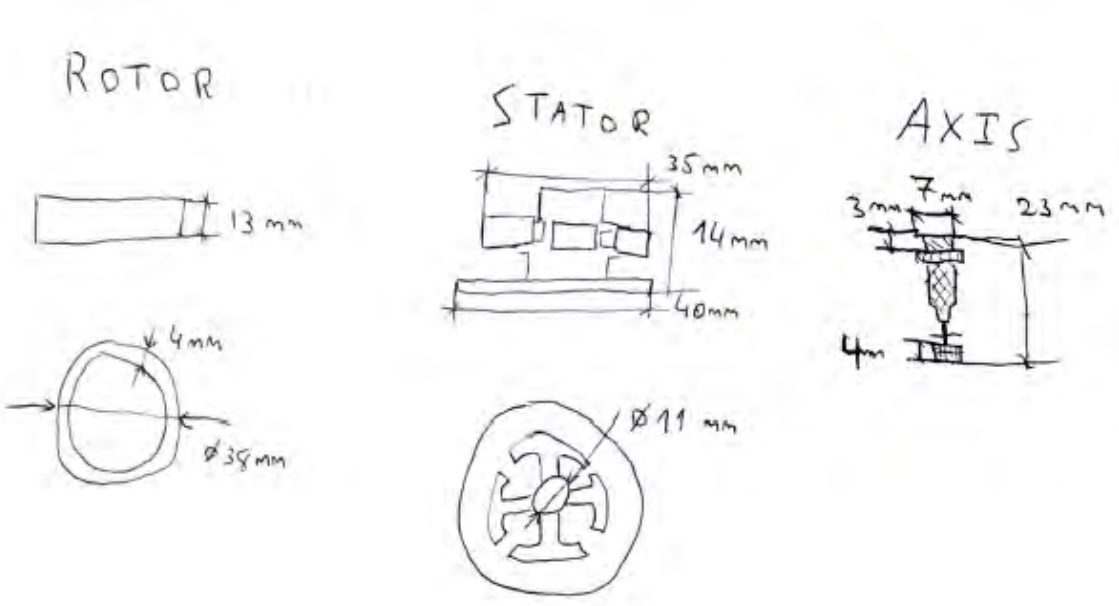

Figure 5.2.1: General sketch of the motor's size

With the general detail as shown in figure 5.2.1 it is now possible to start the design.

The design process followed throughout this project is iterative: certain critical parts that can have unfavorable tolerances are separated and 3-D printed, and once it's made sure that the piece is the desired size and no tolerance errors are found, the next step is carried out.

The first step of the process is to find a rough first idea of the way the rotor, the axis and the bearing are fixed to the casing. For both the rotor and the axis, the idea is to have they fixed by pressure - no special adhesion points needed. To do so, it is imperative to find the appropriate tolerance limit in the sizes to prevent relative movement between rotor and axis, and not add unnecessary strain on the 3-D printed piece.

As for the bearing, the architecture of the fan is duplicated. The bearing, as it did in the fan, sits in a hole in the middle of the stator, which is in turn fixed to the casing by pressure too. For testing purposes two platforms were designed with these critical tolerance-dependent unions. Each platform is a minimalist round piece with just enough material to hold everything in place in order to reduce the waste of 3-D printed material. Once the unions of each part have been proved to work, the rest of the design can be carried out.

Figure 5.2.2: Printed casing tolerance tests

Figure 5.2.2 shows the aforementioned tolerance tests for the rotor, stator and axis/bearing. The part corresponding to the stator has a central piece that goes through the hole in the middle of the motor, and a side has a notch on its side to allow for the cables going to the motor's integrated controller to not be forced into being tensed by going around the edge of the piece. A total of 3 iterations for the stator part were printed, with mostly tolerance errors and problems with the thickness of the bearing wall, which when 3-D printed too thin it had no strength and broke. The rotor part also went through a total of four iterations due to tolerances but the most important change was the following:

Figure 5.2.3: Change in the printed rotor casing

Figure 5.2.3 shows the main advantage of the iterative process: the change of potentially overlooked issues in the design without needing to rework the entire concept of the structure. As you can see, the first version had two walls for the rotor, but the inner wall was dropped off for the final version. This is due to the interaction it had with the stator: the inner wall made contact with it, so it didn't allow for the proper assembly of the two tests, the rotor, the stator and the axis.

The complete casing of the motor is designed by completely covering the rotor, so no further design is needed.

5.2.2 Electrode support

With the casing already designed, the next step is to look at the size requirements and compare them with the current size of the motor casing. The maximum width for the field mill, as per the size requirement, is about 6 cm. For the field mill to work, the electrodes must be symmetrical around the rotating shielding electrodes.

The casing has a diameter of 41 mm. The electrodes must make a circle around the motor's axis, so the total available area is approximately of 2828 mm^2, corresponding to the full circle with a diameter of 6cm. If the electrodes were around the casing, and the shielding electrodes were located atop the motor casing, spinning with it, the available area would be reduced to 1507.17 mm^2. The field mill would probably still work, but as seen in section 3.2, its sensitivity would be drastically decreased. To increase the available area for the electrodes, they have to be moved above or below the motor casing. Figure 5.2.4 shows the proposed solution to this issue. with the rotor casing being reduced in cross-section, the sensing electrodes can take up more of the area previously occupied by an unnecessarily large cross-section.

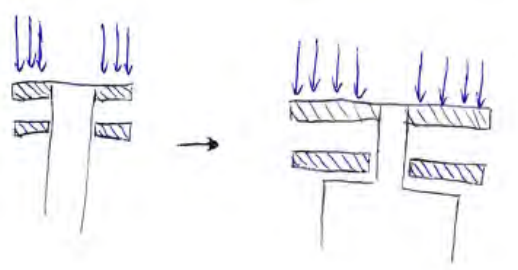

Figure 5.2.4: Visualization of the new distribution.

If the sensing electrodes are moved and increased in area, a new problem arises. The assembly process of the field mill is the following: The mobile rotor piece is inserted in the immobile stator piece in order to have the motor in place and working. If the electrodes have more area than the motor casing, it means the casing can't go through the electrodes.

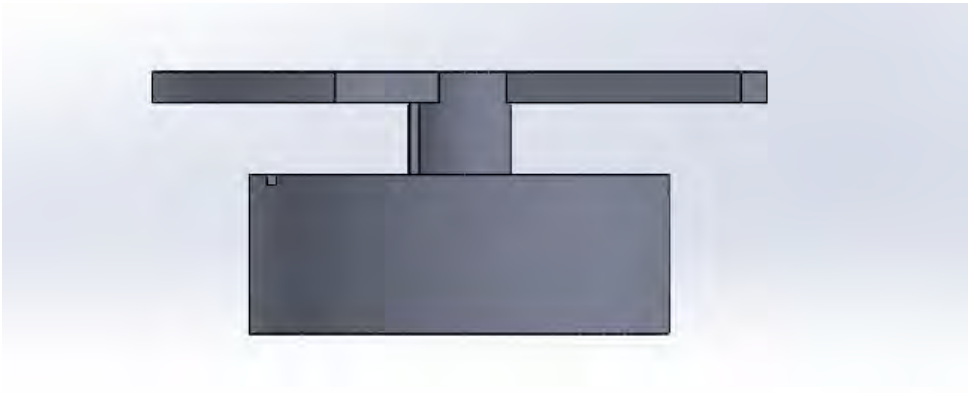

Figure 5.2.5: Support for the grounded shielding electrodes

Figure 5.2.5 shows the solution that allows for more usable area for the sensing electrodes. The shielding grounded electrodes don't need a very thick support connecting them to the rotor casing because the material won't suffer through extreme stresses or strains, so the sensing electrodes can reach further inwards towards the rotation axis.

Also, if the rotating part of the casing has the shielding electrodes (which must have the same dimensions as the sensing electrodes), then the sensing electrodes can't be a single closed piece, or it couldn't be placed under the sensing electrodes. For this reason, the fixed stator structure is separated from the support for the sensing electrodes. The support for the electrodes is assembled after the motor casing in two symmetrical parts.

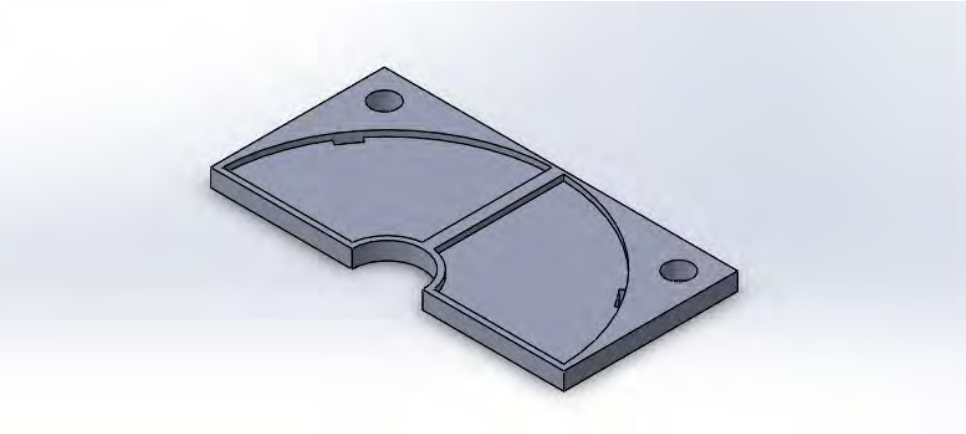

Figure 5.2.6: Support for the sensing electrodes

Figure 5.2.6 shows the design for the support structure of the sensing electrodes. The size of the electrodes is marked with a lower plate thickness. This is done to insulate each electrode from the rest, and to properly distribute the electrodes in a symmetrical continuous pattern.

Now that the structure for the whole field mill is clear, the next step is to put the electrodes in place and find a way to send the signal from them out of the field mill. Aluminium tape is used as the electrodes, since it is lightweight and adaptable to any shape without any complication.

5.2.2.1 Electrode connections

To connect the electrodes to the exterior a copper multicable is used. A copper multicable is a bunch of small copper wires inside rubber protection. The multicables are very malleable and it can be shaped in any way desired. Paired with special holes in the electrode's support (both sensing and grounded shielding), the signal from the electrodes can be accessed from outside the mill. As for the grounding of the shielding electrodes, it is carried out through a graphite brush which presses against the aluminium tape in the sides of the rotor casing, as shown in detail in figure 5.2.7

5.2.2.2 Brush allocation

The graphite brush used to connect the shielding rotating electrode to ground was provided by LRG, and it's a 16mm long brush with a spring at the end. To ensure proper contact while not slowing down the motor with too much friction, the proper allocation for the brush must be taken into account with the design. The brush socket in the external structure of the mill is located at the opposite end of where the motor's cables are accessed, to avoid difficulties in accessing to both the brush and the motor. The same iterative process was followed to find

the appropriate tolerance limits for the brush fitting. A small block with a slot with the brush's measures was printed, and only one iteration was needed.

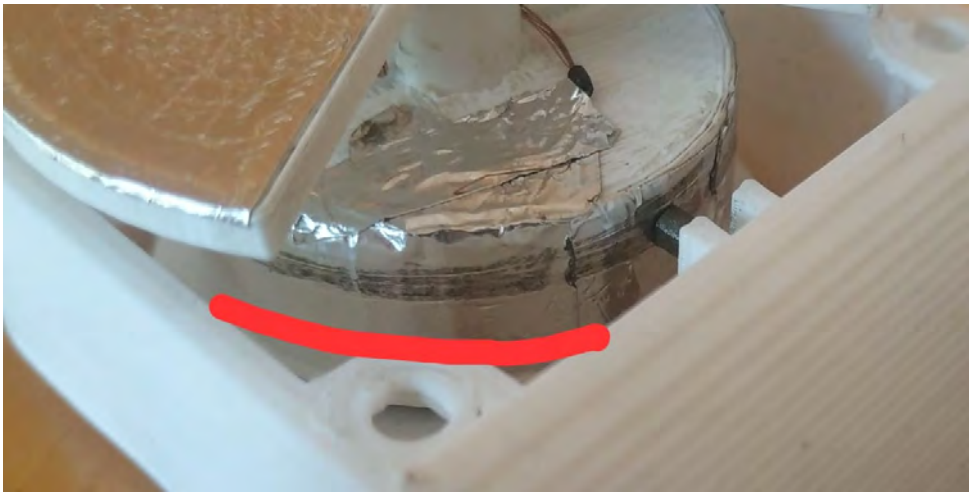

Figure 5.2.7: Detail of the contact area between the brush and the rotor casing

With the connections all made, the final step is to modify the external structure to reduce the aerodynamic impact of the field mill on the aircraft.

5.2.3 External cover of the field mill

An in-depth aerodynamic study of the field mill's impact on the aircraft is considered out of the scope of this project. Nevertheless, an elliptical shape was given to the profile of the field mill's external structure and cover to reduce its influence in the aircraft. Two iterations of this structure were printed. The first iteration was a solid block except for where the motor goes, but the lack of space complicated access to the internal parts and the support for the bearing of the axis broke during dismantling after testing the motor's normal operation. The second iteration was hollow, which makes assembly and disassembly much easier. The hollow structure is shown in figure 5.2.8.

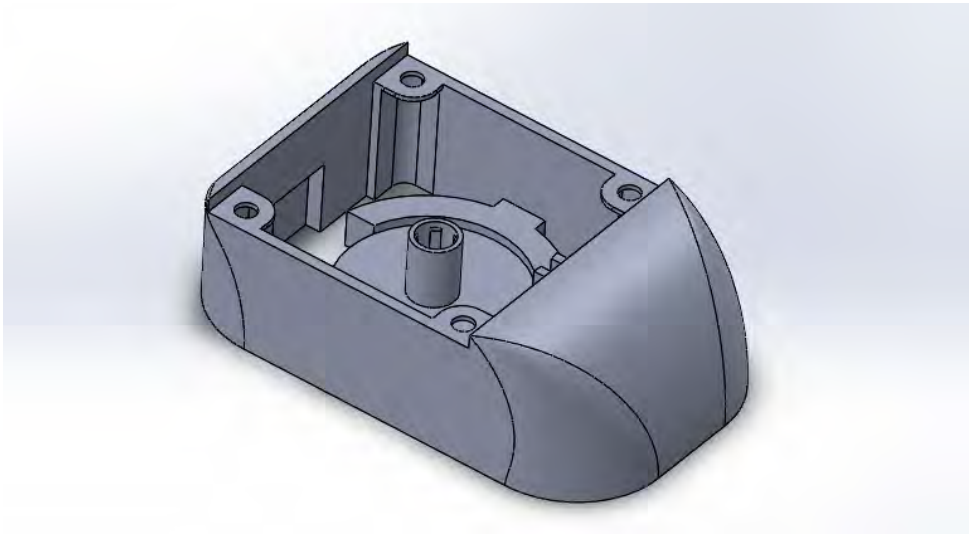

Figure 5.2.8: Final external cover for the field mill, with the allocation for the stator inside

In figure 5.2.8, apart from the elliptical shape of the cover, the means to pin up the sensing electrode support to the external structure is evident. In each corner of the cover a 4mm hole protrudes out from the walls to allow the use of screws to keep all the different parts together.

After every piece is printed, after the electrodes are in place and connected, the electric field mill is finished:

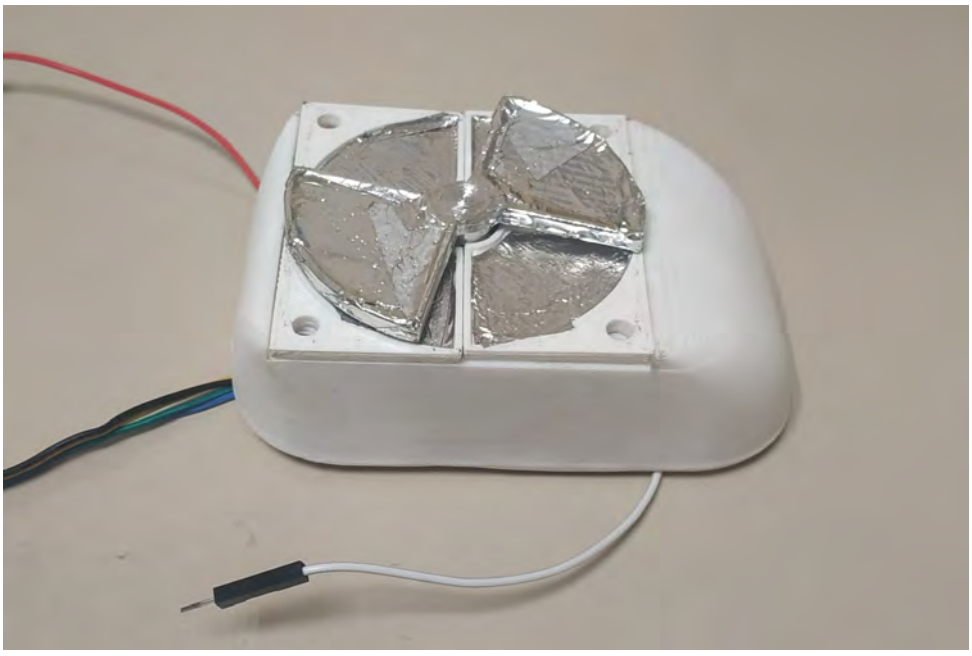

Figure 5.2.9: Finished field mill

6 | Validation & Results

After building the field mill it is imperative to make sure no errors have been made during the process, the field mill is validated.

6.1 Validation process

The validation is done by reading the sensor's output when no electric field is exposed and comparing it to the output when the field mill is exposed to a strong electric field. In the validation process of this project, a simple statically-charged plastic was used.

To measure the output of the field mill an oscilloscope probe is connected between ground and a 4 $M\Omega$ resistor in order to transform the induced current into a difference in potential. The measurements of the oscilloscope probe are shown in figure 6.1.1:

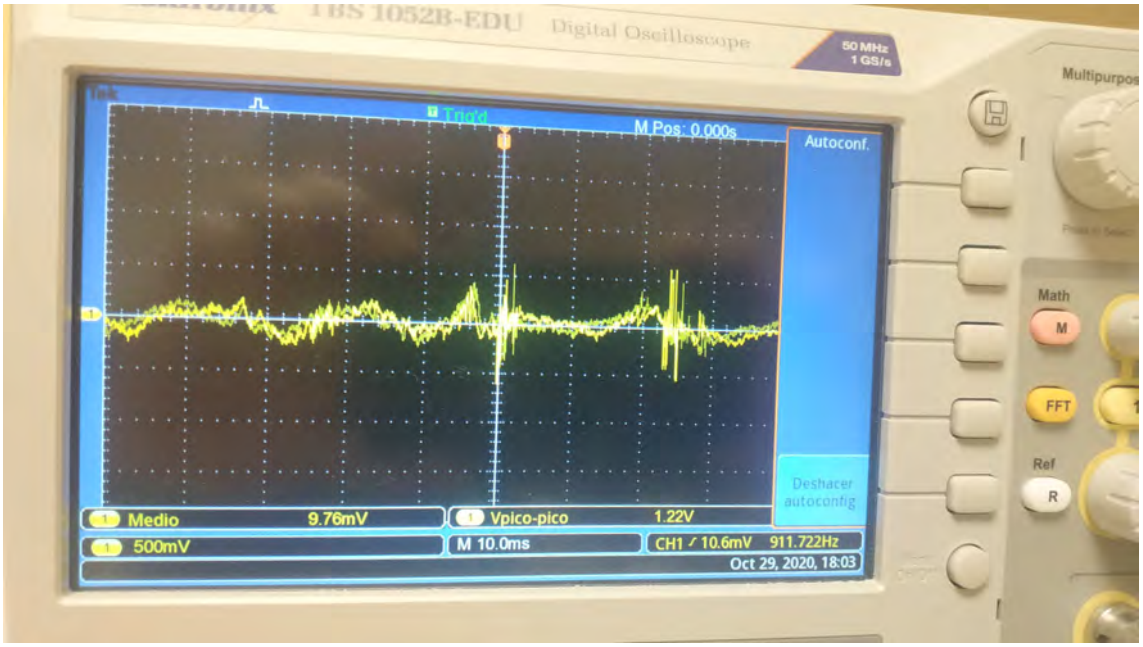

Figure 6.1.1: Oscilloscope screen, measuring the field mill with a resistor while the field mill is not rotating

Clearly the probe receives just noise, and the readings are inappropriate. The reason behind all the noise is the value of the resistor. As mentioned before in section 3.2, the current induced is minimal. With a bigger resistor a bigger signal would be received. But in this situation, the field mill isn't turned on and spinning.

When the field mill is turned on and spun at its maximum rotation speed, the oscillator measurements are:

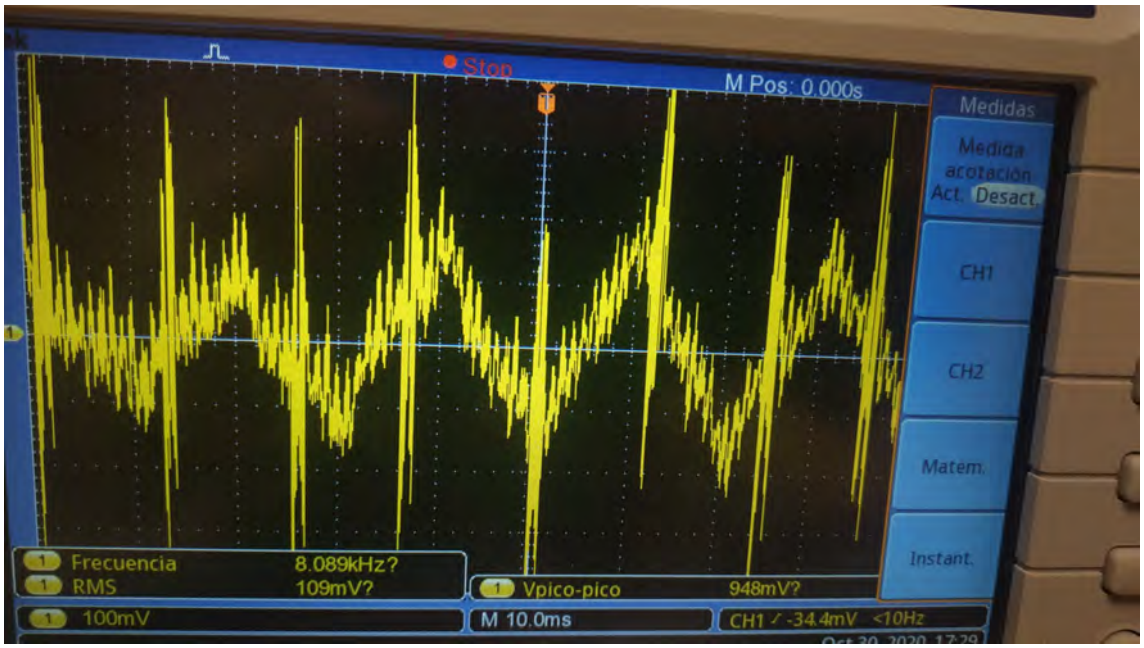

Figure 6.1.2: Oscilloscope screen, measuring the field mill with a resistor while the field mill rotates at maximum RPM

Figure 6.1.2 paints a much different picture than figure 6.1.1. In figure 6.1.2 a clear triangular wave can be seen, with big discontinuities in noise levels at certain points within it. These spikes can be attributed at wrinkles or bumps in the aluminum tape which is in contact with the graphite brush. When said wrinkle or bump hits the brush, its contact with the tape may be inconsistent, so at that point the grounding connection is instantaneously lost, which generates the noise spikes. Nevertheless, the output matches the theoretical output mentioned in section 3.2 and in figure 3.2.1.

With the field mill moving, when a statically charged plastic was drawn near the field mill there was no visible increase in the amplitude of the wave happened as a response. The problem is caused by the fact that the underside of the grounded blocking electrodes wasn't properly covered in the conductive layer of aluminium tape, so the sensing electrodes were picking up the signal from the electrically charged plastic holding the grounded shielding electrodes in place.

Once the shielding electrodes are properly wrapped in aluminium tape, the next step towards

properly visualizing the output of the field mill is to filter out the noise and amplify the signal. To do so, a board with multiple filters and amplifiers was provided by the ***LRG***. With it, the ouptut signal was much more evident.

The first step was to turn the field mill on and see the output of the field mill after filtering and amplifying. The oscilloscope signal is shown in in figure 6.1.3:

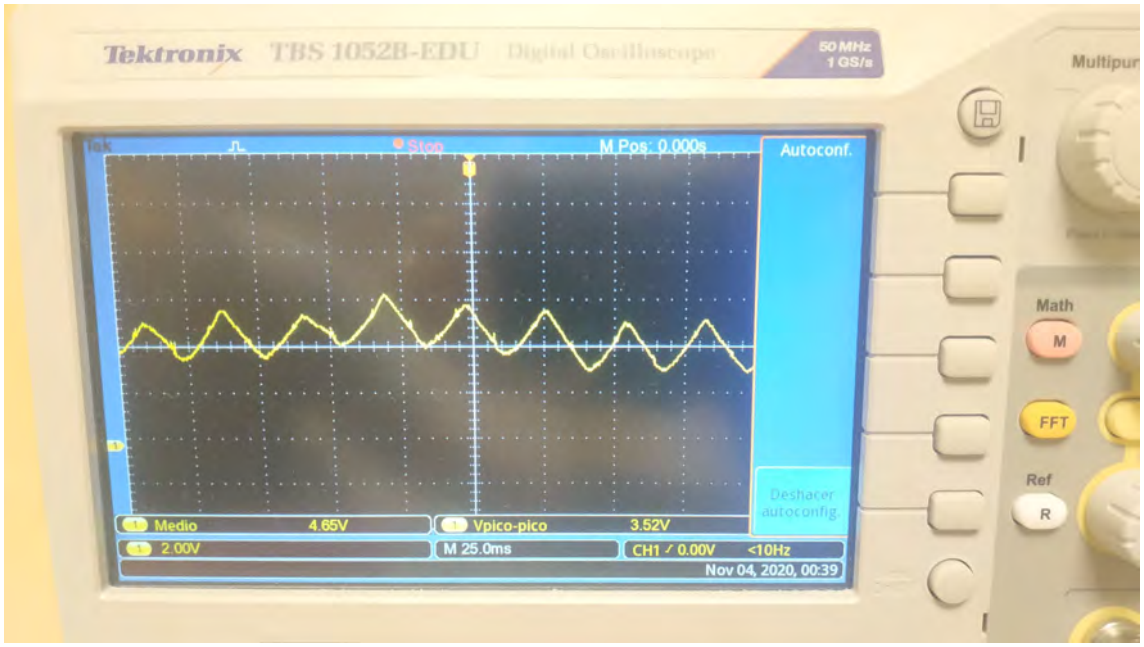

Figure 6.1.3: Oscilloscope screen, measuring the field mill output through the filter and amplifyer.

from first glance it is evident that the triangular signal is practically noise-free. Even the noise spikes of the graphite brush are filtered out. With the ability to properly process the information from the field mill, the final validation step is to see if there are any appreciable changes in amplitude when a statically charged piece of plastic draws near.

Figure 6.1.4 shows the signal when the plastic is close to the field mill. Compared to the measured output when no charge was around in figure 6.1.3, the triangular wave oscillates at a higher voltage, and its amplitude is increased, too.

To properly visualize the effect of bringing the charged plastic closer, the time scale is reduced and the plastic is brought near the field mill and quickly retired again, so that the increase in amplitude can be seen on the screen. Figure 6.1.5 shows the results of this method:

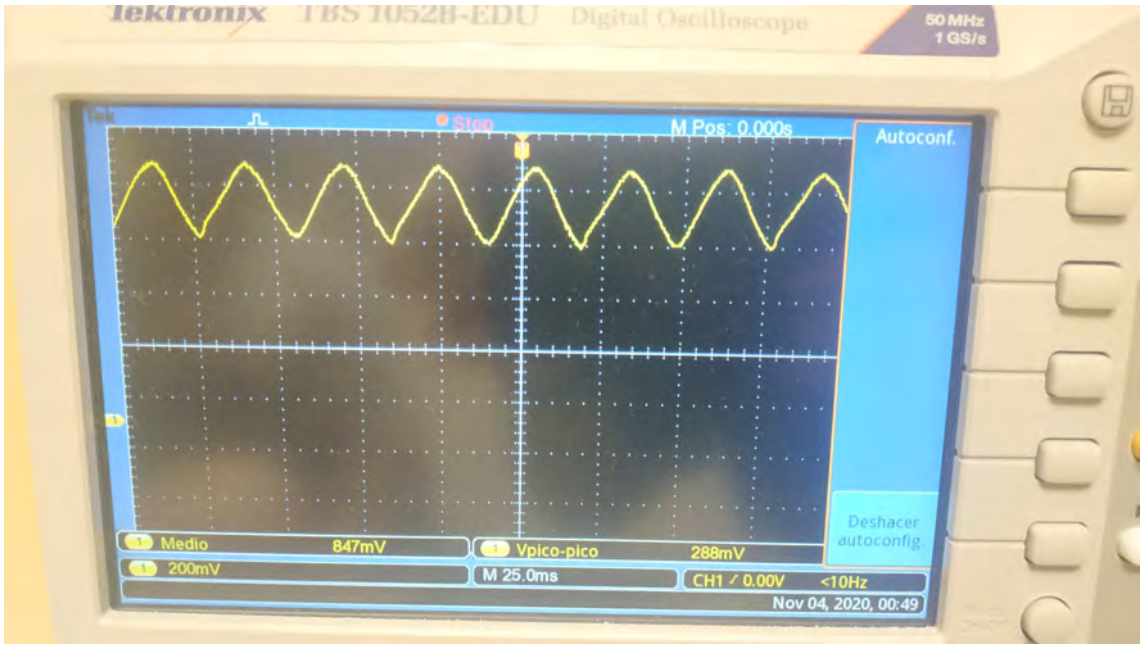

Figure 6.1.4: Oscilloscope screen, measuring the processed field mill output when a charged plastic is near..

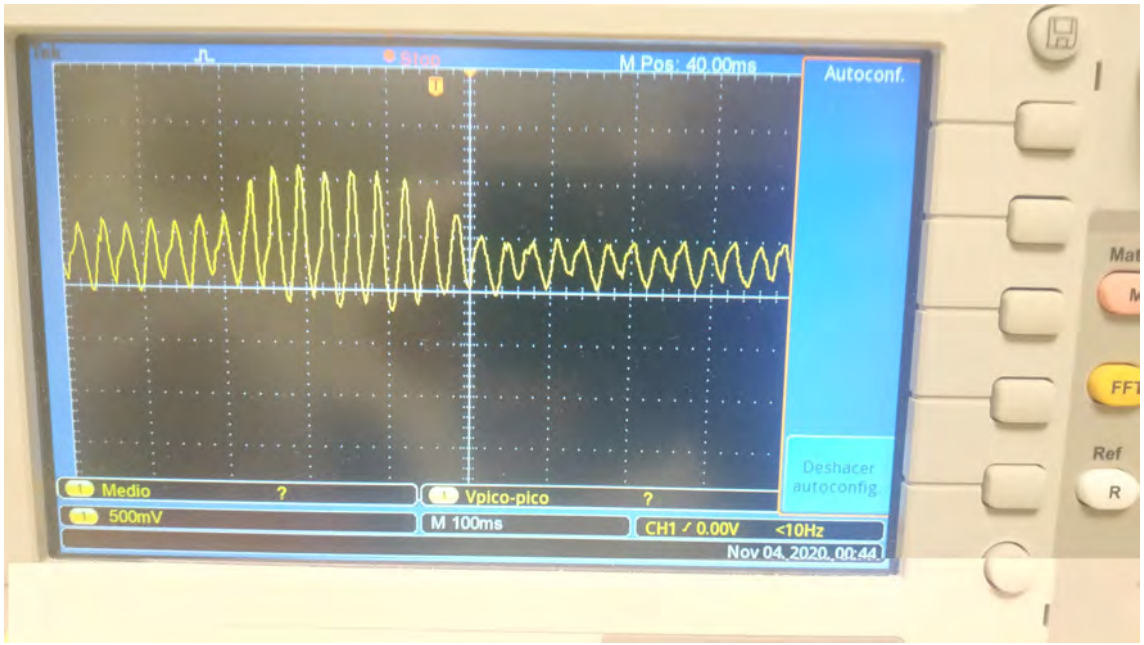

Figure 6.1.5: Oscilloscope screen, measuring the increase in the amplitude of the signal when plastic is brought near and retired.

The result drawn from these experiments is that after proper post-processing of the signal, variations in the electric field can be measured with the designed field mill, so the design in this project can be exploited to infer the amount of charge an aircraft has acquired by measuring the electric field above and below the aircraft, after proper calibration of each field mill.

6.2 Observations

As mentioned in the previous section, the field mill is proven to be usable in the measuring the acquired charge of an aircraft after calibration. However, the structural part of the sensor has some unsolved design flaws. The main design flaw observed during the validation process is the bearing of the brushless DC motor axis. In the disassembled fan, the bearing uses a combination of hydrostatic pressure of pressurized oil inside the bearing, and an external magnet to maintain the rotor and the stator aligned at all times. During the design phase of this project, the hydrostatic oil pressure was not taken into account, and the rotor and stator have to be manually aligned before turning on the motor every time.

Another observed problem in the design is the unreliability of the graphite brush used, and its impact on the functionality of the field mill, since it is a key component of it. As noted in figure 6.1.2, a lot of noise is attributed to it, and the friction it applies onto the rotor casing is so high it can dramatically slow down the motor, especially when the aforementioned alignment is modified. It is also important to note that the pressure applied by the brush can be enough to misalign the rotor and stator, causing further problems.

6.3 Next steps

So, what's next? Critically, before any further action is taken, the bearing of the axis must be reworked to keep proper alignment of the rotor and stator at all times. Currently, pressurizing oil and using its hydrostatic pressure is not viable, so another method has to be studied.

After the bearing is reworked, the other critical part that needs to be addressed is the brush. With the amount of friction it applies lowers the effective rpm regime of the field mill, thus reducing its sensitivity.

After the issues have been resolved, the coefficients of the controllers for each field mill can be checked and adapted accordingly to keep the system stable and synchronized, and then test flights can be performed.

After a successful test flight, the field mill is ready to be used in the measuring of the acquired charge of an aircraft.

7 | Environmental impact

In this project, the electric field mill was built for scientific purposes, so there's no production or commercialization involved. However, a study of the environmental impact of the developed sensor is necessary. This study is limited to the resources used in the construction of the sensor, so no indirect pollution (e.g. electricity used in the elaboration of the documents, or the delivery of the components) is considered in this study.

7.1 Materials used

To develop the sensor, the principal structural material was Polylactid Acid, better known as PLA, a very cheap and common 3-D printing material produced from plants such as the sugarcane, or corn [7]. Apart from the 3-D printed structure,the electrical components used are mostly cables, resistors, an Arduino board, an IMU, and a PCB. In the UAV, the field mill and its electronics are powered by a lithium-ion battery.

7.2 Energy used

The 3-D printer is a machine that heats up a spool of material, in this case the PLA, and uses an extruder to lay this material onto a plate, which is usually heated to allow for proper adhesion of the material. The 3-D printer in the *LRG lab* is the FlashForge Creator 3, and on average it requires a power supply of 500 watts to function. The total printing time, which is provided by the software of the printer [3], totals to approximately 15 hours of 3-D printing. The total energy used is approximately 7.5 kWh. In the location of the *LRG lab* the electricity comes from multiple power plants, and not all of them are renewable. The equivalent pollution per kWh is approximately 0.4 Kg of CO_2 and 75 mg of radioactive waste [9]. So, the total pollution of the printing is about 3 Kg of CO_2 and 562.5 mg of radioactive waste.

7.3 End of life

When the field mill is no longer in use, all the electronic components, including the brushless DC motor, can be salvaged and reused for other projects. The 3-D printed material PLA is biodegradable [7], and it can also be recycled.

8 Conclusions

To reduce an aircraft's tendency to trigger lightning, its net electrical charge must be artificially manipulated. To measure the change in an aircraft's net electrical charge two electrical field mills are required to compare the electric field in opposite directions and calculate the net charge acquired. A field mill is a device which exposes electrodes to an electric field and periodically covers them with grounded shielding electrodes, and the change in the induced charge in the senging electrodes is measured.

The field mill in this thesis is designed by disassembling CPU fans and salvaging their brushless DC motors which already have built-in encoders that allow for simple Arduino boards to control them, and then building a structure around it to house the sensing electrodes and the grounded shielding electrodes.

A PI controller is designed for the synchronization of the motors in section 4.1, and the properties and communication protocols to read the information of the aircraft's attitude sensor is exposed in section 4.2. Their corresponding circuits are developed in section 5.1. The structure housing the motor and the electrodes is explained in section 5.2.

The field mill is proven to have the ability to measure the electric field, although it is not calibrated in this thesis. After passing through a filter and amplifier, a change in the output's amplitude is noticeable when exposed to an electric field.

The next steps are to revise some issues found in section 6.2, and to perform test flights before the field mill is suitable to be used for the measurement of the acquired charge of an aircraft.

9 | Bibliography

[1] Arduino - AboutUs.

[2] Bormatec | Ravensburg | Drohnen.

[3] Creator 3 - FlashForge.

[4] Leyla Asena, Sirel Gür Güngör, and Ahmet Akman. I2C User manual. *International Ophthalmology*, 37(2):391–399, 2017.

[5] Bosch Sensortec. BNO055 datasheet. (November):105, 2014.

[6] M. Goldman, A. Goldman, and R. S. Sigmond. The corona discharge, its properties and specific uses. *Pure and Applied Chemistry*, 57(9):1353–1362, 1985.

[7] Tsuji H. Poly (lactic acid). *Bio-Based Plastics: Materials and Applications,*, pages 171–239, 2013.

[8] R. Giles Harrison and Graeme J. Marlton. Fair weather electric field meter for atmospheric science platforms. *Journal of Electrostatics*, 107(May):103489, 2020.

[9] Grup Jose-Antonio Ortiz and Enginyeria Mec. Tecnologia de Fabricació.

[10] Pulse Width Modulation. Noctua PWM specifications white paper.

[11] C. Pavan, P. Fontanes, M. Urbani, N. C. Nguyen, M. Martinez-Sanchez, J. Peraire, J. Montanya, and C. Guerra-Garcia. Aircraft Charging and its Influence on Triggered Lightning. *Journal of Geophysical Research: Atmospheres*, 125(1):1–15, 2020.

[12] Understanding Space Radiation. Falcon 9 launch weather criteria. *October*, 3:1–7, 2002.

[13] Power Systems. *Air Insulation Prediction Theory and Applications*.

[14] Cape Town and Applied Science September. The Electric Field mill. 1994.

[15] Esaii Upc. Control Automàtic.

[16] Ken Weidman, Chuck; Cummins. Lecture 11 - Thunderstorm electrification.

[17] Ken Weidman, Chuck; Cummins. Lecture 1 - The Global Electric Circuit, 2013.

[18] Ken Weidman, Chuck; Cummins. Lecture 14 - Lightning Phenomenology pt. 1, 2013.